Global NEST Journal, Vol 26, No 10, 06643
Copyright© 2024 Global NEST
Printed in Greece. All rights reserved

Effective removal of calcium and magnesium Ions from boiler feed water using Polyacrylonitrile supported Titanium Tungstovanadate composite ion exchange nanofiber

Ahmed Gameel[1, 2], Hassan A. Farag[2], Dina El-Gayar[2] and Eman M. El-Sayed[3]*
[1]Chemical Engineer, Petrochemicals Company, Alexandria, Egypt.
[2]Chemical Engineering Department, Faculty of Engineering, Alexandria University, Alexandria, Egypt.
[3]Fabrication Technology Research Department, Advanced Technology & New Materials Research Institute (ATNMRI), City of Scientific Research and Technological Applications (SRTA-City), 21934, Alexandria, Egypt.
Received: 16/08/2024, Accepted: 06/09/2024, Available online: 09/10/2024
*to whom all correspondence should be addressed: e-mail: mdr.eman@yahoo.com.
https://doi.org/10.30955/gnj.06643

Graphical abstract

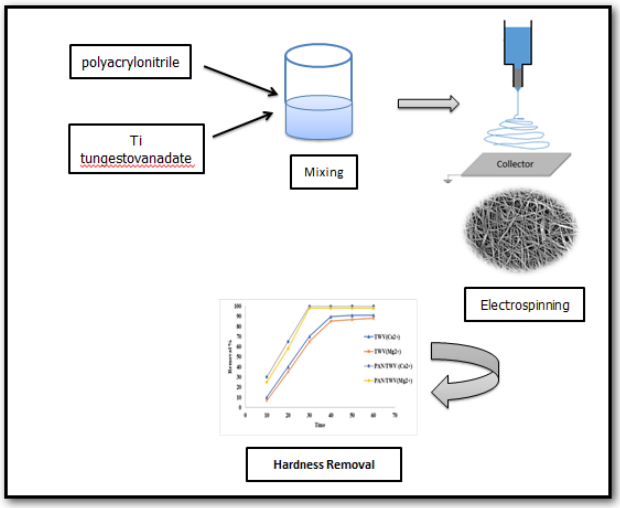

Abstract

The challenge posed by the presence of calcium ions (Ca^{2+}) in process streams is attributed to its adverse effects on the heat transfer efficiency of process equipment. In this study, a novel electrospun nanofibrous composite was synthesized by combining polyacrylonitrile (PAN) with well-dispersed Titanium tungestovanadate (TWV) cation exchanger. Homogeneous precipitation technique was employed to synthesize nano-titanium (IV) tungstovanadate (TWV) cation exchanger. Various synthesis parameters, including reactant volume ratio, amount of precipitating agent and reaction temperature, were optimized to achieve the highest ion exchange capacity (IEC). The prepared ion exchange material exhibited an ion exchange capacity (IEC) of 2.39 meq.g^{-1} for Na^{+} ions. The incorporation of the prepared nanoparticles into nanofibers conferred the sorption capabilities of the composite. The nanofibers' morphologies and structures were analyzed using Fourier transform infrared (FTIR), scanning electron microscopy (SEM), and X-ray diffraction (XRD). Batch sorption experiments were carried out to investigate the sorption properties. Controlled experiments were conducted to investigate the impact of various factors, including solution pH, temperature, dosage, contact time, and the initial concentration of the hard water. The results indicated that the optimum adsorption conditions that gave the highest percentage of removal 99%, 98% for Ca^{2+} and Mg^{2+} ions respectively were 50 mg of adsorbent dosage, 500 ppm of Ca^{2+} and Mg^{2+} solution =7, and a contact time of 30 min at room temperature. The kinetic data were fitted to pseudo second order model. Furthermore, the thermodynamic study suggested that the adsorption on PAN/TWV NF was endothermic and spontaneous.

Keywords: Ion exchange, hard water, polyacrylonitrile, nanoparticles.

1. Introduction

Divalent ions, such as iron, manganese, calcium, and magnesium, contribute to varying degrees of water hardness in both surface and groundwater. Among these, calcium ions (Ca^{2+}) are the most common culprits of water hardness (Park J-S *et al.* 2007; Júnior OK *et al.* 2010; Kim J *et al.* 2019), leading to undesirable mineral precipitation in water supply systems. These occurrences can negatively impact the heat transfer efficiency in process equipment and the separation efficiency of membrane systems employed in water treatment (Kim J *et al.* 2019; Gabrielli C *et al.* 2006; Seo S-J *et al.* 2010; Van Limpt B and Van Der Wal A 2014; Yoon H *et al.* 2016). The presence of Ca^{2+} can induce biocolloids, resulting in excessive precipitation or clogging issues (Sobeck DC and Higgins MJ 2002). Consequently, the complete removal of hardness from water is essential to prevent membrane fouling, as well as to minimize the excessive use of detergent and chelating chemicals in cooling and washing water (Júnior OK *et al.* 2010). Various methods, including thermal evaporation

(Koren A and Nadav N 1994; Shaffer DL *et al.* 2013), ion-exchange (Wiers BH *et al.* 1982), chemical precipitation (Dean JG *et al.* 1972), electrodialysis (Yeon K-H *et al.* 2004), reverse osmosis (RO), and nanofiltration (NF) (Ghizellaoui S *et al.* 2005; Hauck AR and Sourirajan S 1969), have been extensively utilized for the removal of Ca^{2+} from water. However, some of these conventional approaches come with their own set of limitations. Conventional methods for calcium ion (Ca^{2+}) removal, such as chemical precipitation, electrochemical reduction, and certain membrane separation processes, are associated with drawbacks, including the excessive use of chemicals, high energy consumption, and the generation of substantial waste residues that may contribute to secondary pollution (Seo S-J et *al.* 2010; Yoon H *et al.* 2016; Ghizellaoui S *et al.* 2005; Godiya CB *et al.* 2020; Cegłowski M *et al.* 2018; Ghaemi N *et al.* 2015). Electrochemical reduction, in particular, is an expensive process with relatively low efficiency for waste removal.

In contrast, membrane separation and adsorption methods have emerged as promising alternatives. These techniques offer advantages such as ease of membrane/adsorbent fabrication, high selectivity, cost-effectiveness, and the potential for adsorbent reuse (Fu F and Wang Q 2011; Lakherwal D 2014; Ahmed FE *et al.* 2015; Abdullah N 2019; Milagres JL *et al.* 2019). Synthetic polymers and membranes have gained attention for their application in removing Ca^{2+} from industrial wastewater, such as circulating cooling water from boilers or air-conditioning systems. Additionally, these materials can be used to chelate Ca^{2+} and magnesium ions (Motomizu S *et al.* 1992; Chen M *et al.* 2018). Recent research has explored the capabilities of various synthetic polymers and conventional membranes in capturing Ca^{2+} (Xiao S *et al.* 2016). While these methods can effectively remove Ca^{2+}, their application may be limited due to their relatively low adsorption capacity. Polyacrylonitrile (PAN) is recognized as a commonly employed and environmentally stable commercial polymer. It possesses favorable chemical and thermal properties, along with good solubility in organic solvents. The versatility of PAN has led to its widespread use in the electrospinning process for the production of nanofibers. This electrospinning technique allows for the creation of nanofibrous structures, leveraging PAN's properties to generate materials with diverse applications. Nanofibers continue to be an area of intensive research due to their versatility, offering promising solutions in healthcare, energy, environmental protection, and beyond. The have high surface area-to-volume ratio. Nanofibers provide a large surface area, beneficial in applications such as filtration, catalysis, and sensors. Nanofibrous mats have interconnected pores, which can be controlled during fabrication, making them ideal for filtration, tissue engineering, and drug delivery. Despite their fine size, nanofibers can offer high tensile strength, which is important for applications requiring mechanical durability.

In this work, PAN-based nanofibers were prepared by the electrospinning technique. The prepared exchanger was thoroughly characterized to analyze its morphology and chemical composition. Furthermore, its performance in treating water containing Ca^{2+} and Mg^{2+} ions was evaluated.

2. Materials and methods

2.1. Reagents and instrumentation

Titanium (IV) chloride (purity 99%, Bio Basic INC.), Sodium metavanadate (purity 98%, Sigma-Aldrich), sodium tungstate (purity 99%, ACROS Organics) have been used as the raw materials for the synthesis of titanium (IV) tungstovanadate and Urea (purity 99%, Aldrich Chemistry) as precipitating agent. Acrylonitrile (AN) (purity 99%, Sigma-Aldrich), N,N-dimethylformamide (DMF) (99.9+%, Fluka) potassium persulfate (99%, Sigma-Aldrich). All chemicals were used without further purification.

X-ray powder diffraction (XRD, Cu-K radiation, Shimadzu-7000, Kyoto, Japan) was used to determine the crystallographic phase of the prepared samples. Their morphology was examined by scanning electron microscopy (JSM-IT200, USA) combined with energy dispersive X-ray analysis (EDX) for the elements identifications. The microstructure was also observed by JEM-2100 transmission electron microscope (TEM, JEOL, Japan) Fourier transform infrared (FTIR) analysis was done with a Bruker ALFA spectrometer (Bruker Corporation, Ettlingen, Germany).

2.2. Synthesis of Titanium tungstovanadate (TWV) nanoparticles

Titanium tungstovanadate ion exchanger has been synthesized using homogenous precipitation approach using urea as a precipitating agent. The effect of reactants volume ratio, dose of urea and reaction temperature were examined and their impact on the ion exchange capacity of the prepared material was determined. Typically, solutions of 0.1 M titanium (IV) chloride in 0.01 M HCl, 0.1 M sodium metavanadate and 0.1 M sodium tungstate were mixed with different volume ratios, and then urea was added to the reaction mixture. The resulting slurry was then heated to 80 °C and stirring was continued to decompose the precipitating agent. The obtained precipitate was filtered and washed repeatedly with distilled water. The product was dried at 60 °C for 24 hr. Finally, the product was calcinated at 600 °C for 5 hr. The obtained nanoparticles were immersed into 2 M nitric acid with calm stirring to transform the prepared cation exchange into its hydrogenated form. After 24 hr., the cation exchanger was washed with distilled water and dried at 60 °C for 8 hr. In order to determine the chemical and physical properties of the prepared samples, the one which showed the largest IEC for Na^+ ion was selected for further studies and fully characterized.

2.3. Ion Exchange Capacity (IEC)

Ion exchange capacity generally is taken as measure of the hydrogen ion liberated by neutral salt that flow through the ion exchanger. The ion exchange capacities of the different prepared ion exchanger samples were determined by acid-base titration (Roy K *et al.* 2004). Certain weight of the prepared ion exchanger samples in its H^+ form was soaked in 100 mL of 2 M NaCl solution for 12 hr with stirring at ambient temperature using orbital shaker (Yellow line Os10 Control, Germany) to exchange protons with sodium

ions. The ion exchanged was titrated against a standard solution of 0.1M NaOH using phenolphthalein as indicator. The ion exchange capacity (IEC) was calculated using the following equation:

$$IEC\ (meq/g) = VNaOH^{*}\ CNaOH\ /\ Wd \quad (1)$$

Where, V_{NaOH}, C_{NaOH}, and W_d are the volume of NaOH consumed in titration, NaOH concentration, and the weight of the dry sample, respectively.

2.4. Synthesis of polyacrylonitrile nanoparticles

The formation of polyacrylonitrile (PAN) particles involved the dispersion/emulsion polymerization of acrylonitrile (AN) in an aqueous continuous phase, utilizing potassium persulfate (PPS) as the initiator (Boguslavsky L *et al.* 2005). PAN nanoparticles were produced by dissolving 3 ml AN and 30 mg PPS in 100 ml water. The polymerization of AN took place by shaking the vial in a water bath at 60 °C for 6 hours. The resulting homogeneous and viscous solution was then dried at 100 °C for 4 hours.

2.5. Preparation of PAN/TWV composite nanofibers

PAN solutions with different concentration (1, 3, 6% wt./v) were prepared by adding different amount of PAN powder to solvent DMF. The mixtures were stirred under constant magnetic stirring for 24 hours at room temperature in order to obtain homogeneous solution. The preparation of the PAN/TWV composite solution, PAN solution (3 % wt./v %) then mixed with different amount of nano TWV powder that was selected and characterized sample (S-3) with the highest IEC. Various amounts (0.2, 0.4, 0.8 g) of TWV nanoparticles were mixed with PAN solution. Ultrasonication was applied for 15 min to disperse TWV in PAN solution at room temperature before the spinning step.

2.6. Electrospinning of PAN and PAN/TWN composite solution

Electrospinning of both pure PAN and PAN/TWV composite solution was pumped with a syringe pump at a feed rate of (0.3, 0.5, 0.8) ml/h, a voltage (20, 25, 30) KV and the distance between the syringe needle and the receiving plate was (10, 15, 20) cm were adjusted to obtain the optimum nanofibers. The nanofibers were collected on an aluminum foil receiving plate.

2.7. Adsorption performance of the prepared nanofibers:

The optimum fabricated nanofibers that attained the highest IEC were tested as adsorbent matrices for hardness removal from boiler feed water using batch technique. A stock synthetic solution of 500 ppm Ca^{2+} and Mg^{2+} were prepared separately using deionized water. Using deionized water in boiler feed water treatment experiments can indeed affect the results. Deionized water lacks the natural ions, minerals, and impurities found in typical feed water, which can lead to several differences in experimental outcomes. Deionized water presents an idealized environment free from competing ions (such as sodium, chloride, or bicarbonate), which can influence the behavior of the ions being studied (e.g., Ca^{2+} and Mg^{2+}). In real boiler feed water, these competing ions could affect the cation exchange process or overall water chemistry, potentially leading to different removal efficiencies. A certain weight of the prepared nanofibers was added into 100 ml of the Ca^{2+} and Mg^{2+} solutions, followed by shaking at room temperature. 5 ml samples of the water were taken at predetermined intervals and the final Ca^{+2} and Mg^{+2} concentrations were determined using atomic absorption. The influence of different parameters affecting the process as effect of contact time (0-60 min), dosage of the nanofiber (30-80 mg), pH (3-9) was studied.

3. Results and discussions

3.1. Synthesis of nano-Titanium tungstovanadate Ion Exchanger

3.1.1. Impact of reactants mixing volume ratio

Table 1 illustrates the synthesis of Titanium (IV) tungstovanadate using different volume ratios of titanium (IV) chloride, sodium tungstate, and sodium metavanadate at 80 °C, with the addition of 0.3 M urea. It is evident that increasing the volume of tungstate and vanadate ions results in an enhanced ion exchange capacity of the prepared material, as opposed to increasing the concentration of titanium. This can be attributed to the increase in the anionic component responsible for the ion exchange process within the ion exchanger. The optimal volume ratios of Ti:W:V were determined to be 1:2:1, which exhibited the highest ion exchange capacity (IEC) (Nabi SA and Naushad M 2007).

Table 1. Effect of reactants volume ratio on the IEC of the prepared Ti (IV) tungstovanadate:

Sample	Mixing Volume ratio (v/v)			IEC (meq/g)
	Ti (IV) chloride (0.1M)	Sodium tungstate (0.1 M)	Sodium metavanadate (0.1 M)	
S-1	1	1	1	1.7
S-2	1	1	2	2.0
S-3	1	2	1	2.39
S-4	2	1	1	1.8
S-5	1	3	1	2.1
S-6	1	1	3	1.9

3.1.2. Effect of precipitating temperature

The effect of temperature on the IEC of the prepared material was determined using the predetermined optimum reactants ratio (1:2:1) at different temperatures. Table 2 showed that the IEC of the produced ion exchangers were increased with increasing the reaction temperature, where the maximum IEC of 2.39 meq.g^{-1} was obtained at a temperature of 80 °C. However, further

increase in the reaction temperature has a negative effect on the IEC. This may be due to the increase in urea dissociation producing carbonate ions that foul the prepared exchanger surface and decrease its exchange capacity (Shaw WH and Bordeaux JJ 1955).

Table 2. Effect of temperature on the ion exchange capacity of TWV:

Temperature, (˚C)	IEC, (meq. /g)
40	1.5
60	2.1
80	2.39
90	2.15

3.1.3. Effect of precipitating agent dose

To optimize the dosage of the precipitating agent (urea), several samples of titanium tungstovanadate ion exchanger were prepared with varying amounts of urea in relation to the weight of titanium chloride used. The urea dosage ranged from 0 to 0.6 M. As indicated in Table 3, the exchange capacity of the prepared material exhibited an increase with increasing urea dosage, followed by a subsequent decrease. The optimal ion exchange capacity (IEC) value was achieved with 0.3 M urea. The decrease in IEC can be attributed to urea hydrolysis and the formation of a carbonate precipitate (Boguslavsky L *et al.* 2005).

Table 3. Effect of urea dose on the IEC of Ti (IV) tungstovanadate:

Urea, (M)	IEC, (meq./g)
0.0	1.2
0.2	1.6
0.3	2.39
0.6	1.9

3.2. Characterization of the prepared titanium tungstovanadate sample with the highest IEC (S-3):

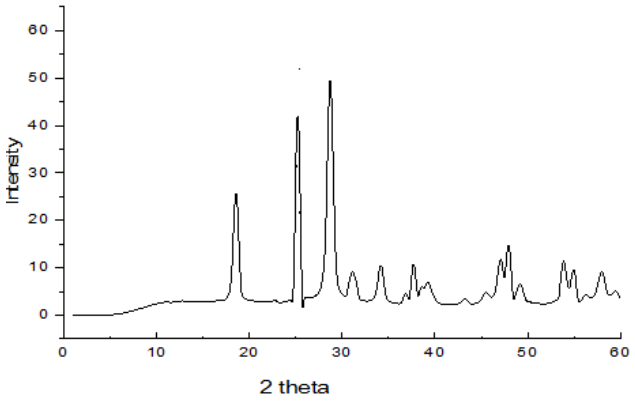

Figure 1. X-ray diffraction pattern of titanium (IV) tungstovanadate (S-3).

Figure 1 represents the x-ray pattern of the best prepared sample (S-3) that attained the highest ion exchange capacity. The X-ray spectrum confirmed that the heteropoly acid salt is crystalline in nature and it revealed number of peaks at different 2θ values confirming the presence of Ti, W and V and O. The presence of anatase is discarded in our sample, whereas the rutile phase of TiO_2 was predominant with diffraction peaks at 2θ = 18.2 º,25.3º, 37.7º,47.8, 53.9ºand 58.6º.

Morphological characterization of S-3 was performed using SEM. Figure 2 indicates that the prepared hetropoly acid salt is spherical in shape and in nano scale with an average diameter 59.13 nm.

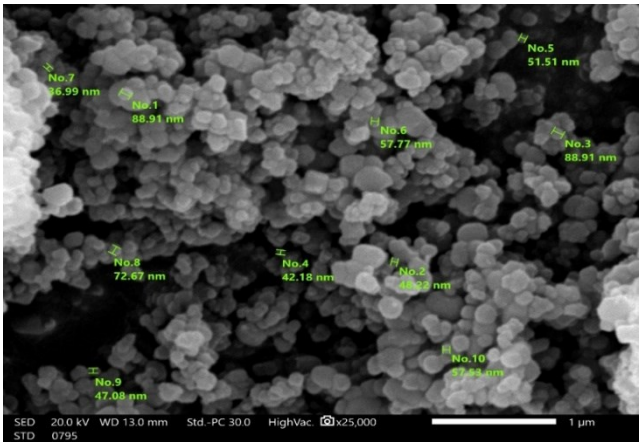

Figure 2. SEM micrograph of prepared titanium tungstovanadate (S-3).

FTIR of the best prepared sample results is shown in Figure 3. The strong and broad peak at 3398 cm^{-1} corresponds to the presence of interstitial water and hydroxyl groups. A sharp peak at 1631 cm^{-1} corresponds to deformation vibration of free water molecules (Al-Othman Z and Naushad M 2011). A small peak at 2368.12 cm^{-1} was due to Ti-O vibrations (Busani T and Devine R 2005). However, the peak at 1000 cm^{-1} shows the presence of vanadate ion. And the broad band in the region of 806-508 cm^{-1} indicated the existence of Ti-O bond (Zheng L *et al.* 2016) and may be assigned to metal oxide bond formation (Socrates G 1980). Hence, from the IR analysis, it can be deduced that the materials are composed mainly of a mixture of titanium tungsten oxide and titanium vanadium oxide.

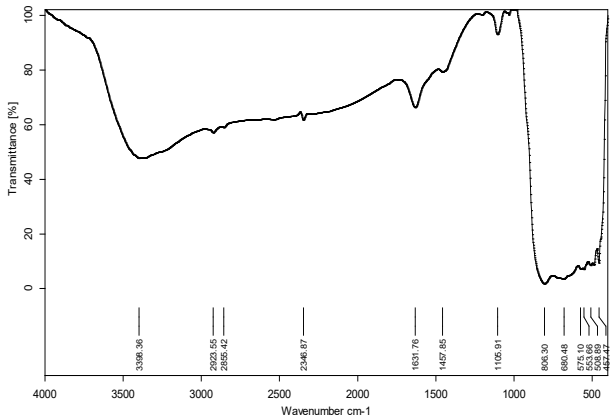

Figure 3. FTIR of the prepared titanium (IV) tungstovanadate (S-3).

3.3. Fabrication of PAN and PAN/TWV nanofibers

Effect of PAN Concentration

Polymer concentration is an important operational parameter in the electrospinning process, which influences fiber morphology significantly. The formation of the fibers is inhibited in the solutions with high concentrations due to their high viscosity (Beachley V and Wen X 2009). The high viscosity makes the solutions extremely difficult to flow

through the syringe needle to form nanofibers under an electrostatic force (Ding B *et al.* 2002). Therefore, appropriate solution concentration becomes one of the key parameters to optimize the final electrospinning fibers. During this experiment, the effect of polymer concentration on spinnability and fiber diameter was investigated by changing the concentration percentage of the PAN in DMF. Different concentrations, such as 1%, 3% and 6% wt./v. are taken in a set of experiments. Different concentrations, such as other parameters, such as applied voltage, feed rate and distance between tip-collector are kept fixed at 20 KV, 0.5 ml/hr. and 15 cm, respectively.

Figure 4 showed the SEM image of pure PAN nanofibers electrospun with concentrations of 1%, 3%, and 6% wt. %, respectively. At 1% concentration, the obtained fibers were nonuniform and some beads were observed due to the lack of force balance among the electrostatic repulsion, surface tension, and viscoelastic force (Fong H *et al.* 1999; Huebner A 1970). By increasing the concentration to 3 wt. %, the morphology of nanofibers was changed from a beaded fiber to a uniform fiber structure and the fiber average diameter was 80 nm (Bakar SSS *et al.* 2019). At 6 wt.% which consider as high concentrations, resulting in larger average diameter of nanofibers because of the inability to maintain the flow of the solution at the tip of the needle (Ki CS *et al.* 2005) and due to their higher viscosity resistance (Pham QP *et al.* 2006). Therefore, based on fiber morphology and uniformity of fiber diameter distribution, 3 wt.% is kept fixed for a further studies.

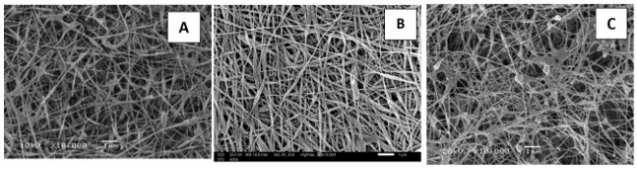

Figure 4. SEM microstructures of pure PAN nanofibers fabricated at a concentration of (A) 1%, (B) 3%, and (C) 6% wt.% (applied voltage = 20 KV., feed rate= 0.5 ml/hr. and tip-to-collector distance =15cm).

3.3.1. Fabrication of PAN/TWV nanofibers

PAN was dissolved in DMF (3% wt./v) and mixed using a magnetic stirrer at room temperature then a certain weight (0.2, 0.4, 0.8 gm) of the best prepared TWV nanoparticles sample (S-3) with the highest IEC was added to the previous solution.

a. Effect of TWV amount

The effect of TWV dosage on the diameter and homogeneity of the formed nanofibers was studied under a constant voltage of 20 kV, a spinning distance of 15 cm, and a feed rate of 0.5 ml/h. The SEM images in Figure 5 revealed that increasing the TWV amount decreased fiber uniformity and caused bead defects. This is attributed to the excessive TWV dissolved in the PAN solution, which increases ionic strength and disrupts the balance among surface tension, viscoelastic, and electrostatic forces. Therefore, 0.2 g of TWV was found to facilitate the formation of uniform PAN fibers and was selected for further studies.

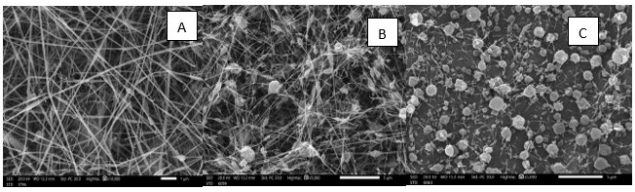

Figure 5. SEM images of PAN/TWV nanofibers at different TWV NPs dosages dosages (A) 0.2g , (B) 0.4 g (C) 0.8 g (applied voltage 20KV, tip-to-collector distance 15 cm and feed rate 0.5 ml/h.)

b. Effect of applied voltage

Within the electrospinning process, applied voltage is the crucial factor. It provides surface charge on the electrospinning jet and affects nanofiber diameter. Increasing the applied voltage would cause the polymer jet to discharge more forcefully, resulting in a rise in drawing tension (Macossay J *et al.* 2007). However, very high voltages may facilitate nanofibers at larger diameters due to more polymer ejection (Demir MM *et al.* 2002). In addition, bead formations can occur at high voltages (Deitzel JM *et al.* 2001). Different spinning voltages (20, 25, and 30 kV) were simulated respectively. According to Figure 6, higher bead formation can be observed when the applied voltage was increased. This was due to the increase in the electrostatic repulsive force on the liquid jet which then increased the formation of beads on fibers. Therefore 20 kV was the optimum voltage for polymer fiber fabrication because smooth interconnected fibers were produced at this voltage with the smallest diameter.

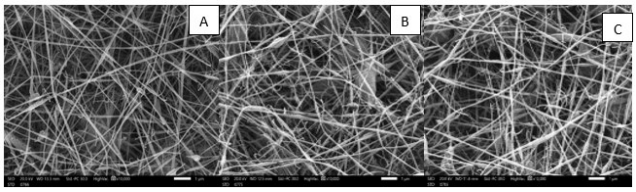

Figure 6. SEM images of PAN/TWV nanofibers with different applied voltage = (A) 20 KV, (B) 25 KV (C) 30 KV.

c. Effect of tip-to-collector working distance

The distance between the metallic needle tip and collector plays an essential role in determining the morphology of an electrospun nanofiber. Hence, a critical distance needs to be maintained to prepare smooth and uniform electrospun nanofibers. affects the nanofiber morphologies and diameter because of their dependence on the evaporation rate, deposition time, and instability interval or whipping (Matabola K and Moutloali R 2013). The influence of the spinning distance on the morphology and diameter of the electrospun PAN/TWV nanofibers is evaluated at feed rate 0.5 ml/h and applied voltage 20 KV. In this study, the three receiving distances between the spinneret and the collector were 10, 15, 20 cm respectively.

From Figure 7 it can be observed that, at working distance 10 cm, beads and non-uniform fiber are observed as the formed nanofibers will not have enough time to solidify before reaching the collector (Buchko CJ *et al.* 1999). With an increase in the distance, the average fiber diameter decreased from 75.8 to 63 nm with improved uniformity. This is attributed to the complete solvent evaporation , and more stretching and thinning, which favors the formation of thinner fibers (Ding W *et al.* 2010; Ziabari M *et al.* 2010).

When the working distance increased to 20 cm the uniformity of the fibers decreased and some cracks were observed in the PAN/TWV nanofibers.

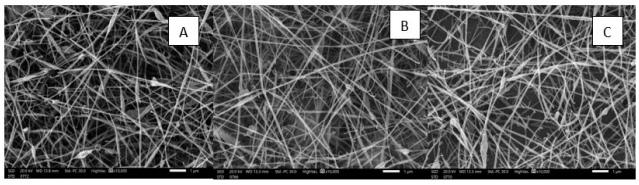

Figure 7. SEM images of PAN/TWV nanofibers at different tip to collector distance. (A) 10 cm (B) 15 cm (C) 20 cm (Applied voltage = 20 KV and feed rate = 0.5 ml/h)

d. Effect of feed rate

It has been observed that the feed rate of the polymer solution significantly affects the morphology of polymer fibers (Deitzel JM *et al.* 2001). It is essential to maintain a minimum flow rate of the spinning solution, ensuring it is sufficient for fiber formation. Typically, a lower flow rate is favored because it allows the polymer solution within the metallic needle ample time for polarization. Additionally, the lower flow rate facilitates adequate time for solvent evaporation from the forming fiber, resulting in a dry fiber on the collector (Zong X *et al.* 2002; Yuan X *et al.* 2004).

In contrast, higher flow rates can lead to the formation of beaded fibers. This is attributed to the combination of low stretching forces and a shortened drying time for the fiber before it reaches the collector (Zuo W *et al.* 2005). Figure 8 shows the SEM microstructures of the PAN/TWV nanofibers fabricated at constant working distance of 15 cm, a fixed applied voltage of 20 kV, and different flow rates 0.3, 0.5 and 0.8 ml/h respectively. With increasing feed rate from 0.3 to 0.5 ml/h, the average diameter is decreased from 75 to 63 nm (Megelski S *et al.* 2002). When the flow rate increased to 0.8 ml/h, the nanofibers with thick diameter was formed were unable to dry completely before reaching the collector and higher bead defects were therefore observed (Zuo W *et al.* 2005).

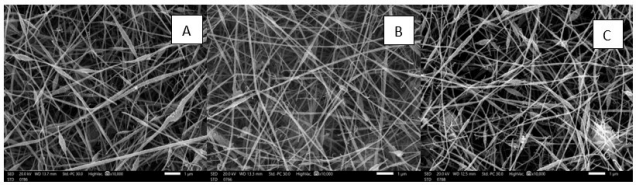

Figure 8. SEM images of PAN/TWV nanofibers at different feed rate (a) 0.3 (B) 0.5 (c) 0.8 ml/hr. (Applied voltage =20 KV and tip to collector distance= 15 cm)

3.4. Characteristics of PAN/TWV composite nanofiber:

a. X-ray diffraction

Figure 9 shows the XRD diffraction patterns of electrospun PAN/TWV Composite NF. We could see that there was a diffractive peak where 2θ was 16.9, which corresponded with PAN crystal. Which confirms the presence of PAN and an additional peak also observed at 25.52 due to incorporation of TWV with PAN polymer. Very sharp peaks occurred between 20 and 30°, were associated with successful TWV grafting on the PAN polymer This shows that TWV are well distributed in the PAN matrix, and this filler does not affect the crystal structure, it only changes the connection between the two phases and improves interfacial compatibility (Zadeh ZE *et al.* 2021).

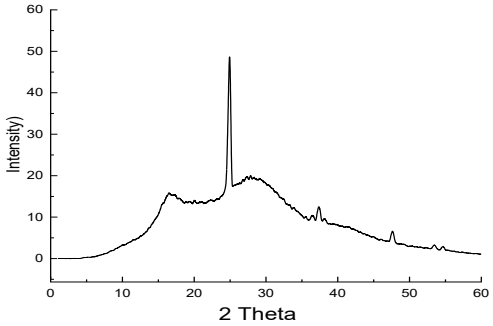

Figure 9. X-ray diffraction pattern of PAN/TWV composite nanofiber

b. Infrared Spectroscopy (FTIR)

FT-IR nanofibers were tested by a Fourier Transform infrared spectrometer. Figure 10 illustrates the FTIR spectrum of PAN/TWV composite nanofiber.

The FTIR spectrum of the PAN/TWV nanocomposite ion exchanger revealed sharp peak at 2926 cm^{-1} was mapped to C-H (García Vera YE *et al.* 2019), absorption peaks of nitrile (–C≡N) group at around 2240 cm^{-1}, The peak at 1627 cm^{-1} was assigned to C=C, the peak at 1027 cm^{-1} can be attributed to the C–C asymmetric stretching vibration of the aromatic group (Strankowski M *et al.* 2016; Wang S *et al.* 2021).The bands at 985 cm^{-1}, 738 cm^{-1} and 543 cm^{-1} may be due to tungstate and metal-oxide groups present in the material and the peaks at 831 cm^{-1} were due to presence of WO_4^{2-} which confirms the impregnation of Titanium tungstate over the PAN film.

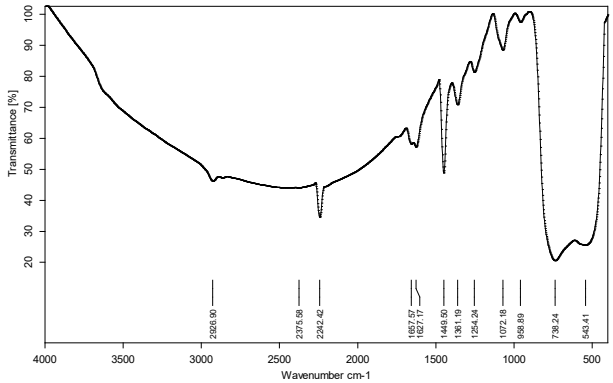

Figure 10. FTIR of the prepared PAN/TWV composite nanofiber

3.5. Adsorption performance evaluation:

Batch adsorption studies were carried out to investigate the Ca^{+2} and Mg^{+2} ions adsorption. The parameters affecting the adsorption process such as dose, pH and time were studied.

3.5.1. Batch Experiments for hardness removal using TWV NPs and PAN/TWV composite NF:

a. Effect of contact time

The study examined the influence of contact time on the sorption of Ca^{+2} and Mg^{+2} ions onto titanium tungstovanadate NPs and PAN/TWV Composite NF, and the findings are presented in Figure 11. Experiments were

performed by taking 100 ml hard water to two different glass bottles. The first one contains approximately 0.5 g of TWV NPs and the second one contains 50 mg of PAN/TWV nanofibers and the mixture of each sample was stirred for varying time periods from (0-60 min).

The results depicted in the figure demonstrate that the percentage of calcium and magnesium removal increases as the contact time extends, reaching equilibrium within 40 mins with TWV NPs and 30 mins with PAN/TWV NF. Subsequently, the removal efficiency of hardness exhibits a gradual increase until it reaches a state of equilibrium, likely indicating that the active sites on the sorbent become saturated with calcium and magnesium ions (Cetin G 2014). Moreover, by using PAN/TWV NF reached equilibrium before TWV NPs, where The main reason for the fast stage is the plenty of free active sites on PAN/TWV nanofiber.

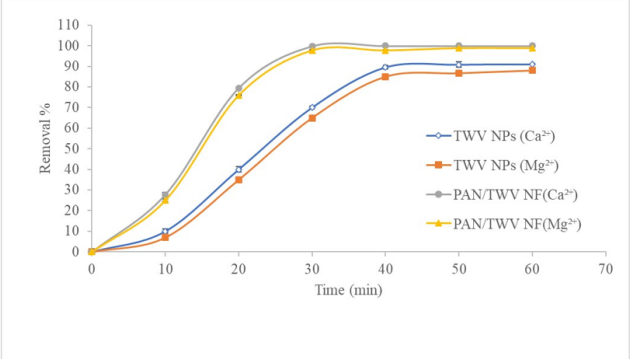

Figure 11. Effect of contact time on the sorption of Ca^{2+} and Mg^{2+} using TWV NP and PAN/TWV NF (initial conc. = 500 ppm; solution volume = 100 mL, temperature = 25 °C; agitation speed= 200 rpm; pH = 7).

b. Effect of Ion Exchanger Dose

To determine the optimum and equilibrium amount of adsorbent for all adsorption experiments, a series of adsorption studies were carried out by changing adsorbent dose of the TWV NPs in the range (0.2-1 g), the mixture was stirred for 60 min. The solution is then filtered and analyzed to determine the concentrations of Ca^{2+} and Mg^{2+}. Additionally, varying amounts of PAN/TWV nanofibers (30, 50, and 80 mg) are used to identify the optimal dosage.

According to the results obtained in Figure 12, the removal efficiency of calcium and magnesium hardness increases with rising amount of the dose (Ho YS and McKay G 2000). It was provides a great ion exchange sites to replace. From this result, it was found that, the %Removal of Ca^{2+}, Mg^{2+}. increases with adsorption dose up to 0.2 g of TWV NPs and 50 mg for PAN/TWV NF and after that it remains almost constant for all materials (Elkady M *et al.* 2014).

However, increasing the adsorbent dose did not result in a significant increase in Ca2+ and Mg2+ removal. This suggests that the total available surface area was not enhanced, likely due to the aggregation of adsorption sites and/or the adsorbate surface not being fully accessible for adsorption (Mittal H *et al.* 2016; Biswal SK *et al.* 2020). The optimum value was 50 mg, higher than that the weight becomes ineffective because the arrival of saturation state (Ravi VP *et al.* 1998).

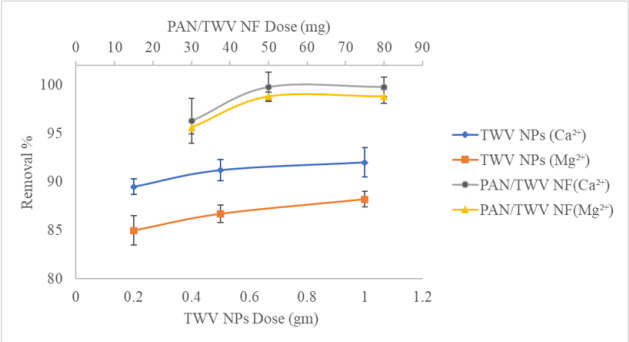

Figure 12. Effect of ion exchange dosage (initial conc. = 500 ppm; solution volume = 100 mL, temperature = 25 ± 2°C; agitation speed = 200 rpm; pH = 7).

c. Effect of solution pH

The pH of the solution has a significant effect on affinity of the prepared ion exchange for calcium and magnesium ions. The initial pH range (3-9). During the study of the effect of pH on adsorption process, other affecting parameters were constant.

The effect of pH on removal efficiency is shown in Figure 13. The maximum uptake capacity occurred at pH =7 (Abd Aziz NI 2019). An increase in pH beyond 7 can trigger the hydrolysis of metallic ions, thereby causing a decline in the biosorption process. Conversely, at lower pH values, the reduction in Ca^{2+}, Mg^{2+} ion removal may be attributed to the competition between H^{+} ions and Ca^{2+}, Mg^{2+} ions in the ion exchange process on the prepared cation exchanger (Saeed A *et al.* 2005).

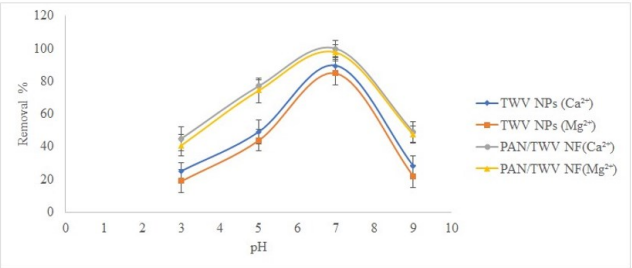

Figure 13. Removal efficiency of TWV NPs and PAN/TWV NF at different pH values (initial conc. = 500 ppm; solution volume = 100 mL, temperature = 25 ± 2°C; agitation speed= 200 rpm).

3.6. Comparison between the sorption performances of TWV nanoparticles and PAN/TWV composite nanofiber:

Batch adsorption studies were carried out to investigate the Ca^{2+} and Mg^{2+} adsorption by using TWV NPs and PAN/TWV NF. The parameters affecting the adsorption process which have been previously investigated in adsorption using TWV nanoparticles. It is clearly observed that the of Ca^{2+} and Mg^{2+} removal is improved by using PAN/TWV composite nanofiber over pure TWV nanoparticles. PAN/TWV NFs is recorded the maximum percentage of Ca^{2+} and Mg^{2+} removal of is 99.9% and 98.8%, respectively. In conclusion, the impregnation of TWV NPs on the PAN NFs showed significant improvement of the adsorption rather than pure TWV NPs. This result indicated that the adsorption capacities of the PAN/TWV composite nanofibers and TWV nanoparticles depended primarily on the surface area and the pore size of the

adsorbents. The porous PAN/TWV nanofibers exhibited the highest efficiency for the removal of Ca^{2+} and Mg^{2+} ions.

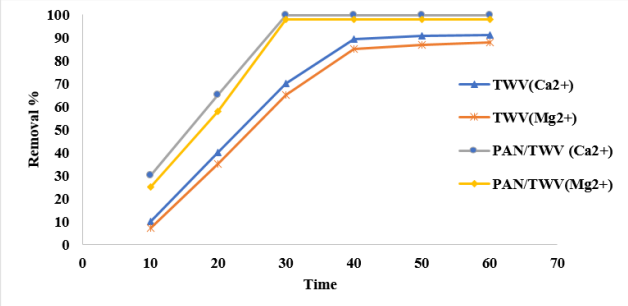

Figure 14. Removal efficiency of Ca^{2+} and Mg^{2+} ions using the prepared TWV NPs and PAN/TWV NF

3.7. Kinetic studies

Kinetic experiments were made by using 100 mL of Calcium solutions and Magnesium solutions with initial concentration 500 ppm were prepared separately and adjusted to the suitable pH value at room temperature. Samples were taken at different time intervals (0-60 min). The adsorption data of PAN/TWV composite nanofiber was fitted by applying various adsorption kinetics models such as, pseudo-first order and pseudo second order.

a. Pseudo-first-order reaction kinetic

Simple linear equation for pseudo-first-order reaction kinetic is given below:

$$\ln (q_e - q_t) = \ln q_e - k_1 t \quad (2)$$

Where, k_1 is the rate constant of the first-order adsorption, q_t is the amount of metal adsorbed at time 't' (mg/g) and q_e is the amount of metal adsorbed at saturation (mg/g).

Plot of ln (q_e - q_t) versus t allows calculation of the rate constant k_1 and qe for calcium and magnesium removal (Figure 16).

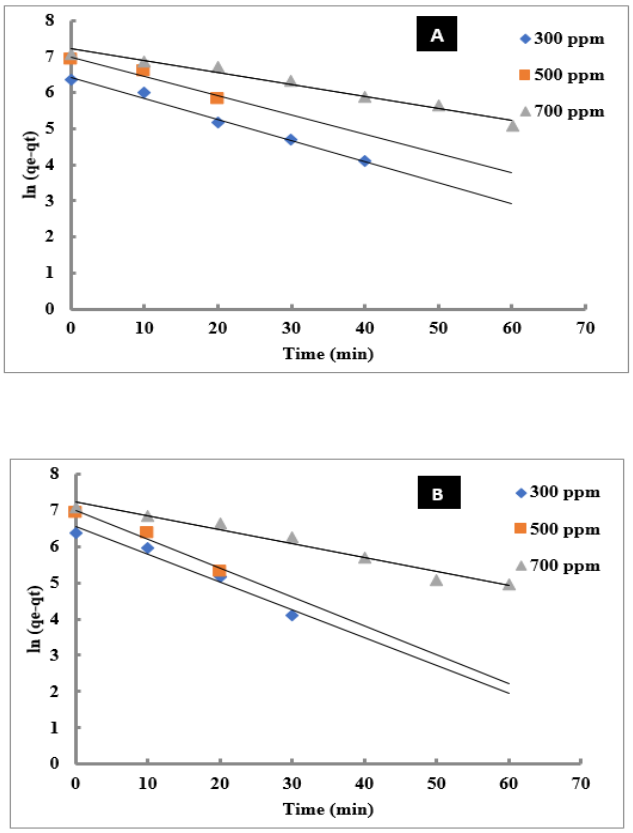

Figure 15. Pseudo-first-order reaction kinetics A) Ca^{2+} B) Mg^{2+} ions on PAN/TWV NF. (Adsorbent= 50 mg, pH=7, Temp=25)

Table 4. Comparison of adsorption rate constants, experimental and calculated q_e values for the pseudo-first- reaction kinetics of removal of Ca^{2+} and Mg^{2+} using PAN/TWV NF.

Sample	Initial Conc. (mg/l)	q_e *experimental (mg/g)*	K_1 (min^{-1})	q_e *Calculated* (mg/g)	R^2
Ca^{2+}	300	600	-0.00128	705.28	0.96
	500	988	-0.00133	1168.29	0.96
	700	1160	-0.00064	1382.29	0.95
Mg^{2+}	300	598	-0.00097	621	0.95
	500	999	-0.00087	1071	0.97
	700	1100	-0.00055	1347	0.94

Table 5. Comparison of adsorption rate constants, experimental and calculated q_e values for the pseudo-second- reaction kinetics of removal of Ca^{2+} and Mg^{2+} using PAN/TWV NF.

Sample	Initial Conc. (mg/l)	q_e *experimental (mg/g)*	K_2 (g/mg min)	q_e *Calculated* (mg/g)	R^2
Ca^{2+}	300	600	0.00024	666	0.96
	500	988	0.00162	1111	0.96
	700	1160	0.000625	1240	0.95
Mg^{2+}	300	598	0.00021	625	0.96
	500	999	0.00016	1115	0.98
	700	1100	0.00024	1428	0.95

b. Pseudo-second-order reaction kinetic:

Pseudo-second-order reaction kinetic can be expressed as:

$$t/q_t = 1/k_2 q_e^2 + t/q_e \quad (3)$$

Where, k_2 (g/mg.min) is the pseudo-second-order rate constant, q_e the amount adsorbed at equilibrium and qt is the amount of metal adsorbed at time 't'. Similar to the pseudo-first-order reaction kinetic, q_e and k_2 can be determined from the slope and intercepts of plot t/q_t versus t.

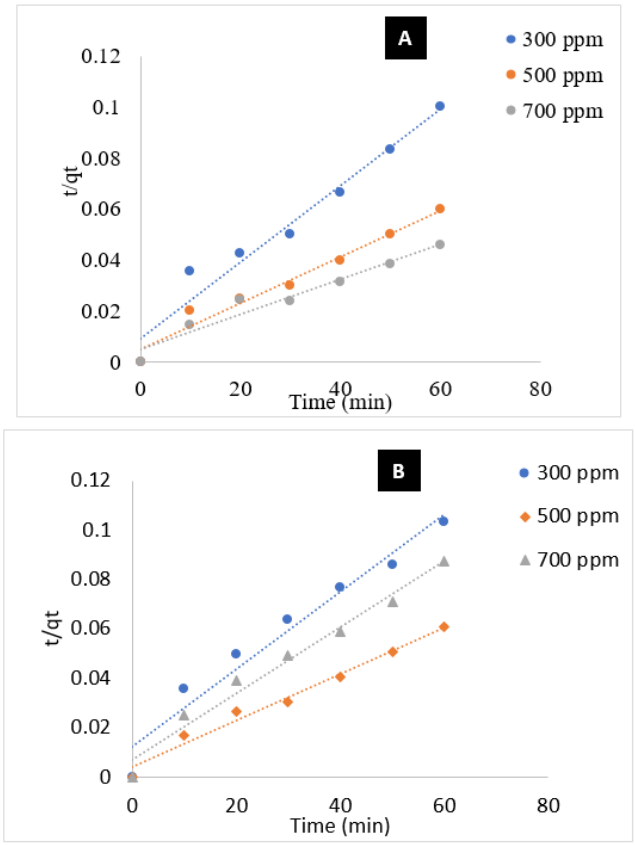

Figure 16. Pseudo-second-order reaction kinetics A) Ca^{2+} B) Mg^{2+} ions on PAN/TWV NF. (Adsorbent= 50 mg, pH=7, Temp=25)

From the two previous tables, which summarize the calculated rate constants (k_1 and k_2), adsorbed amounts of calcium and magnesium per unit mass of PAN/TWV composite NF (qe) and linear regression correlation coefficients (R^2) for pseudo-first- and -second-order reaction kinetics. It was clear that, in pseudo-second-order reaction kinetic, calculated values of qe are closer to the experimental values for metal ions calcium and magnesium. Furthermore, correlation coefficients are higher for second order kinetic studies. This confirms that, the sorption of metal ions calcium and magnesium on the prepared ion exchangers composite nanofiber follows the pseudo second order kinetic model (Namasivayam C and Sureshkumar M 2008).

3.8. Thermodynamic studies:

The apparent thermodynamic parameters enthalpy change (ΔH^o) and entropy change (ΔS^o) for calcium and Magnesium sorption onto PAN/TWV composite nanofiber at different initial metal ion concentrations are calculated from the slopes and intercepts of the linear variation of $\ln(K_d)$ vs. 1/T by the equation (4) (Argun ME 2008).

$$\ln K_d = (\Delta S°/R) - (\Delta H°/RT) \quad (4)$$

The distribution coefficient K_d was calculated using the following equation:

$$k_d = \frac{qe}{Ce} \quad (5)$$

Where, R is the universal gas constant, 8.314 $J.mol^{-1}\,K^{-1}$ and T is the absolute temperature in Kelvin. The free energy (ΔG^o) for the specific sorption is calculated by using the following equation:

$$\Delta G° = \Delta H° - T\Delta S° \quad (6)$$

The computed thermodynamic sorption parameters ΔH^o and ΔS^o from the plots of $\ln K_d$ versus 1/T as shown in Figure 17. The values of ΔH^o and ΔS^o of the adsorption process were, respectively, obtained from the slope and intercept.

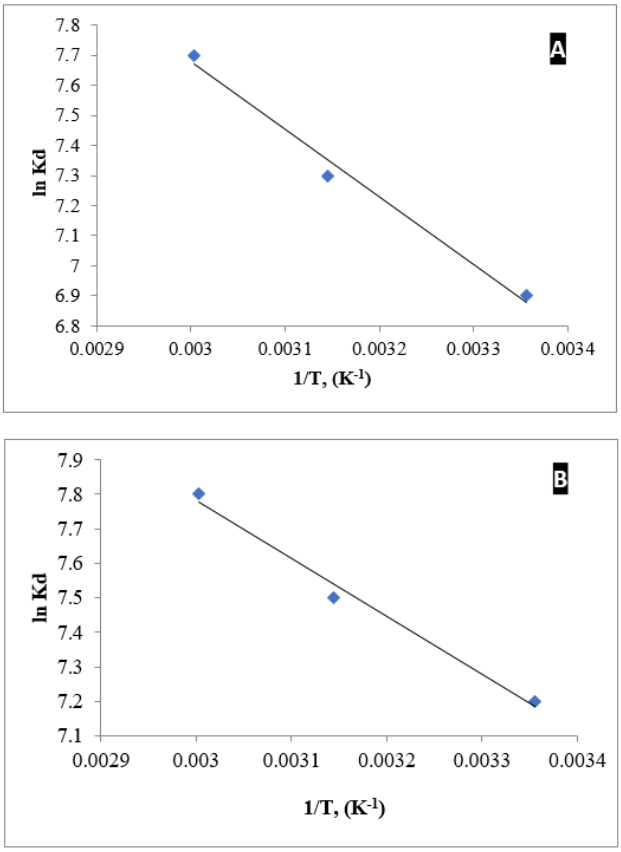

Figure 17. Thermodynamic parameters for A) Ca^{2+} b) Mg^{2+}ions sorption using PAN/TWV NF.

4. Conclusions

Cation exchange in boiler treatment plays a critical role in improving water quality by removing scale-forming ions such as calcium (Ca^{2+}) and magnesium (Mg^{2+}). This process helps prevent scaling, corrosion, and other operational issues in boilers, thus enhancing efficiency and extending the lifespan of equipment. Nanotitanium (IV) tungstovanadate, an inorganic cation exchanger, was successfully synthesized using the homogenous precipitation method and subjected to characterization. The most favorable volume ratios of Ti:W:V were determined to be 1:2:1, resulting in the highest ion exchange capacity. The material demonstrated a sodium ion exchange capacity of 2.39 meq g^{-1}. The prepared ion exchange material demonstrated an ion exchange capacity (IEC) of 2.39 meq.g-1 for Na+ ions. Incorporating the nanoparticles into the nanofibers imparted sorption capabilities to the composite. The morphologies and structures of the nanofibers were analyzed using Fourier transform infrared (FTIR) spectroscopy, scanning electron microscopy (SEM), and X-ray diffraction (XRD). Batch sorption experiments were conducted to evaluate the

sorption properties. Controlled experiments examined the impact of various factors, including solution pH, temperature, dosage, contact time, and initial concentration of hard water. Additionally, the nanofibers were easily separable from the solution and demonstrated high reusability over multiple cycles, indicating their potential for effective wastewater treatment applications.

The influence of various adsorption conditions on removal efficiency was investigated. Results showed that PAN/TWV composite nanofibers could effectively remove Ca^{2+} and Mg^{2+} ions, with optimal conditions achieving removal efficiencies of 99% for Ca^{2+} and 98% for Mg^{2+}. These optimal conditions included 50 mg of adsorbent, 500 ppm of Ca^{2+} and Mg^{2+} solutions, a pH of 7, and a contact time of 30 minutes at room temperature. Additionally, the kinetic data fit well with the pseudo-second-order model. Thermodynamic studies suggested that the adsorption of Ca^{2+} and Mg^{2+} on PAN/TWV nanofibers was endothermic and spontaneous. The Future Challenges that we will consider in our future work is the regeneration efficiency as the use of chemical regenerants (e.g., sodium chloride) poses environmental challenges, necessitating the development of more sustainable regeneration methods. In addition improving the longevity and effectiveness of ion exchange materials to withstand harsh operating conditions is crucial. Top of Form

Funding

This research received no external funding.

Conflicts of Interest

The authors declare no conflict of interest.

Statement of data availability

The datasets generated during and/or analysed during the current study are available from the corresponding author on reasonable request.

References

Abd Aziz NI. (2019). Optimization of pH and contact time of media in removing calcium and magnesium from groundwater. *International Journal of Integrated Engineering*. 11(9):063–72.

Abdullah N, Yusof N, Lau W, Jaafar J and Ismail A. (2019). Recent trends of heavy metal removal from water/wastewater by membrane technologies. *Journal of Industrial and Engineering Chemistry*. **76**:17–38.

Ahmed FE, Lalia BS and Hashaikeh R. (2015). A review on electrospinning for membrane fabrication: Challenges and applications. *Desalination*. **356**:15–30.

Al-Othman Z, Naushad M. (2011). Organic–inorganic type composite cation exchanger poly-o-toluidine Zr (IV) tungstate: preparation, physicochemical characterization and its analytical application in separation of heavy metals. *Chemical Engineering Journal*. **172**(1):369–75.

Argun ME. (2008). Use of clinoptilolite for the removal of nickel ions from water: kinetics and thermodynamics. *Journal of Hazardous Materials*. **150**(3):587–95.

Bakar SSS, Foong KM, Halif NA, Yahud S, editors. (2019). Effect of solution concentration and applied voltage on electrospun polyacrylonitrile fibers. *IOP Conference Series: Materials Science and Engineering*; IOP Publishing.

Beachley V, Wen X. (2009). Effect of electrospinning parameters on the nanofiber diameter and length. *Materials Science and Engineering: C*. **29**(3):663–8.

Biswal SK, Panigrahi GK and Sahoo SK. (2020). Green synthesis of Fe2O3-Ag nanocomposite using Psidium guajava leaf extract: An eco-friendly and recyclable adsorbent for remediation of Cr (VI) from aqueous media. *Biophysical Chemistry*. **263**:106392.

Boguslavsky L, Baruch S and Margel S. (2005). Synthesis and characterization of polyacrylonitrile nanoparticles by dispersion/emulsion polymerization process. *Journal of Colloid and Interface Science*. **289**(1):71–85.

Buchko CJ, Chen LC, Shen Y, Martin DC. (1999). Processing and microstructural characterization of porous biocompatible protein polymer thin films. *Polymer*. **40**(26):7397–407.

Busani T, Devine R. (2005). Dielectric and infrared properties of TiO2 films containing anatase and rutile. *Semiconductor Science and Technology*. **20**(8):870.

Cegłowski M, Gierczyk B, Frankowski M, Popenda Ł. (2018). A new low-cost polymeric adsorbents with polyamine chelating groups for efficient removal of heavy metal ions from water solutions. *Reactive and Functional Polymers*. **131**:64–74.

Cetin G. (2014). Removal of hardness of earth alkaline metals from aqueous solutions by ion exchange method. *International Scholarly Research Notices*. 2014.

Chen M, Xue M, Xu H, Zhang X, editors. (2018). The control of the Ca2+ concentration in the water treatment of the central air conditioner. *IOP Conference Series: Earth and Environmental Science*. IOP Publishing.

Dean JG, Bosqui FL and Lanouette KH. (1972). Removing heavy metals from waste water. *Environmental Science & Technology*. **6**(6):518–22.

Deitzel JM, Kleinmeyer J, Harris D, Tan NB. (2001). The effect of processing variables on the morphology of electrospun nanofibers and textiles. *Polymer*. **42**(1):261–72.

Demir MM, Yilgor I, Yilgor E, Erman B. (2002). Electrospinning of polyurethane fibers. *Polymer*. **43**(11):3303–9.

Ding B, Kim H-Y, Lee S-C, Lee D-R, Choi K-J. (2002). Preparation and characterization of nanoscaled poly (vinyl alcohol) fibers via electrospinning. *Fibers and Polymers*. **3**:73–9.

Ding W, Wei S, Zhu J, Chen X, Rutman D, Guo Z. (2010). Manipulated electrospun PVA nanofibers with inexpensive salts. *Macromolecular Materials and Engineering*. **295**(10):958–65.

Elkady M, El-Sayed E, Farag H and Zaatout A. (2014). Assessment of novel synthetized nanozirconium tungstovanadate as cation exchanger for lead ion decontamination. *Journal of Nanomaterials*. 2014:1-.

Fong H, Chun I, Reneker DH. (1999). Beaded nanofibers formed during electrospinning. *Polymer*. **40**(16):4585–92.

Fu F and Wang Q. (2011). Removal of heavy metal ions from wastewaters: a review. *Journal of Environmental Management*. **92**(3):407–18.

Gabrielli C, Maurin G, Francy-Chausson H, Thery P, Tran T, Tlili M. (2006). Electrochemical water softening: principle and application. *Desalination*. **201**(1–3):150–63.

García Vera YE, Dufo-López R and Bernal-Agustín JL. (2019). Energy management in microgrids with renewable energy sources: A literature review. *Applied Sciences*. **9**(18):3854.

Ghaemi N, Madaeni SS, Daraei P, Rajabi H, Zinadini S, Alizadeh A, *et al.* (2015). Polyethersulfone membrane enhanced with iron oxide nanoparticles for copper removal from water: Application of new functionalized Fe3O4 nanoparticles. *Chemical Engineering Journal*. **263**:101–12.

Ghizellaoui S, Chibani A and Ghizellaoui S. (2005). Use of nanofiltration for partial softening of very hard water. *Desalination*. **179**(1–3):315–22.

Godiya CB, Sayed SM, Xiao Y and Lu X. (2020). Highly porous egg white/polyethyleneimine hydrogel for rapid removal of heavy metal ions and catalysis in wastewater. *Reactive and Functional Polymers*. **149**:104509.

Hauck AR and Sourirajan S. (1969). Performance of porous cellulose acetate membranes for the reverse osmosis treatment of hard and waste waters. *Environmental Science & Technology*. **3**(12):1269–75.

Ho YS and McKay G. (2000). The kinetics of sorption of divalent metal ions onto sphagnum moss peat. *Water Research*. **34**(3):735–42.

Huebner A. (1970). Disintegration of charged liquid jets: Results with isopropyl alcohol. *Science*. **168**(3927):118–9.

Júnior OK, Gurgel LVA and Gil LF. (2010). Removal of Ca (II) and Mg (II) from aqueous single metal solutions by mercerized cellulose and mercerized sugarcane bagasse grafted with EDTA dianhydride (EDTAD). *Carbohydrate Polymers*. **79**(1):184–91.

Ki CS, Baek DH, Gang KD, Lee KH, Um IC, Park YH. (2005). Characterization of gelatin nanofiber prepared from gelatin–formic acid solution. *Polymer*. **46**(14):5094–102.

Kim J, Jain A, Zuo K, Verduzco R, Walker S, Elimelech M, *et al.* (2019). Removal of calcium ions from water by selective electrosorption using target-ion specific nanocomposite electrode. *Water Research*. **160**:445–53.

Koren A and Nadav N. (1994). Mechanical vapour compression to treat oil field produced water. *Desalination*. **98**(1–3):41–8.

Lakherwal D. (2014). Adsorption of heavy metals: a review. *International Journal of Environmental Research and Development*. **4**(1):41–8.

Macossay J, Marruffo A, Rincon R, Eubanks T, Kuang A. (2007). Effect of needle diameter on nanofiber diameter and thermal properties of electrospun poly (methyl methacrylate). *Polymers for Advanced Technologies*. **18**(3):180–3.

Matabola K, Moutloali R. (2013). The influence of electrospinning parameters on the morphology and diameter of poly (vinyledene fluoride) nanofibers-effect of sodium chloride. *Journal of Materials Science*. **48**:5475–82.

Megelski S, Stephens JS, Chase DB and Rabolt JF. (2002). Micro-and nanostructured surface morphology on electrospun polymer fibers. *Macromolecules*. **35**(22):8456–66.

Milagres JL, Bellato CR, Ferreira SO, Guimarães LdM, Tonon GJdP and Bolandini A. (2019). Simultaneous removal process of divalent metal and anionic and cationic dyes by layered reconstruction with hydrocalumite intercalated with dodecyl sulfate. *Colloids and Surfaces A: Physicochemical and Engineering Aspects*. **582**:123890.

Mittal H, Maity A and Ray SS. (2016). Gum karaya based hydrogel nanocomposites for the effective removal of cationic dyes from aqueous solutions. *Applied Surface Science*. **364**:917–30.

Motomizu S, Oshima M, Matsuda S-Y, Obata Y, Tanaka H. (1992). Separation and determination of alkaline-earth metal ions as UV-absorbing chelates with EDTA by capillary electrophoresis. Determination of calcium and magnesium in water and serum samples. *Analytical Sciences*. **8**(5):619–25.

Nabi SA, Naushad M. (2007). Synthesis and characterization of a new inorganic cation-exchanger—Zr (IV) tungstomolybdate: Analytical applications for metal content determination in real sample and synthetic mixture. *Journal of Hazardous Materials*. **142**(1–2):404–11.

Namasivayam C, Sureshkumar M. (2008). Removal of chromium (VI) from water and wastewater using surfactant modified coconut coir pith as a biosorbent. *Bioresource technology*. **99**(7):2218–25.

Park J-S, Song J-H, Yeon K-H .and Moon S-H. (2007). Removal of hardness ions from tap water using electromembrane processes. *Desalination*. **202**(1–3):1–8.

Pham QP, Sharma U, Mikos AG. Electrospinning of polymeric nanofibers for tissue engineering applications: a review. Tissue engineering. 2006;12(5):1197-211.

Ravi VP, Jasra RV and Bhat TS. (1998). Adsorption of phenol, cresol isomers and benzyl alcohol from aqueous solution on activated carbon at 278, 298 and 323 K. *Journal of Chemical Technology & Biotechnology: International Research in Process, Environmental AND Clean Technology*. **71**(2):173–9.

Roy K, Mohapatra P, Rawat N, Pal D, Basu S, Manchanda V. (2004). Separation of 90Y from 90Sr using zirconium vanadate as the ion exchanger. *Applied radiation and isotopes*. **60**(5):621–4.

Saeed A, Iqbal M, Akhtar MW. (2005). Removal and recovery of lead (II) from single and multimetal (Cd, Cu, Ni, Zn) solutions by crop milling waste (black gram husk). *Journal of Hazardous Materials*. **117**(1):65–73.

Seo S-J, Jeon H, Lee JK, Kim G-Y, Park D, Nojima H, *et al.* (2010). Investigation on removal of hardness ions by capacitive deionization (CDI) for water softening applications. *Water Research*. **44**(7):2267–75.

Shaffer DL, Arias Chavez LH, Ben-Sasson M, Romero-Vargas Castrillón S, Yip NY and Elimelech M. (2013). Desalination and reuse of high-salinity shale gas produced water: drivers, technologies, and future directions. *Environmental Science & Technology*. **47**(17):9569–83.

Shaw WH, Bordeaux JJ. (1955). The decomposition of urea in aqueous media. *Journal of the American Chemical Society*. **77**(18):4729–33.

Sobeck DC and Higgins MJ. (2002). Examination of three theories for mechanisms of cation-induced bioflocculation. *Water Research*. **36**(3):527–38.

Socrates G. (1980). *Infrared Characteristic Group Frequencies John Wiley & Sons*. Ltd: Chichester.

Strankowski M, Włodarczyk D, Piszczyk Ł and Strankowska J. (2016). Polyurethane nanocomposites containing reduced graphene oxide, FTIR, Raman, and XRD studies. *Journal of Spectroscopy.* 2016.

Van Limpt B and Van Der Wal A. (2014). Water and chemical savings in cooling towers by using membrane capacitive deionization. *Desalination*. **342**:148–55.

Wang S, Chi H, Chen L, Li W, Li Y, Li G, *et al.* (2021). Surface functionalization of graphene oxide with polymer brushes for improving thermal properties of the polymer matrix. *Advances in Polymer Technology*. 2021:1–11.

Wiers BH, Grosse RJ and Cilley WA. (1982). Divalent and trivalent ion exchange with zeolite A. *Environmental Science & Technology*. **16**(9):617–24.

Xiao S, Luo X, Peng Q, Deb H. (2016). Effective removal of calcium ions from simulated hard water using electrospun polyelectrolyte nanofibrous mats. *Fibers and Polymers*. **17**:1428–37.

Yeon K-H, Song J-H and Moon S-H. (2004). A study on stack configuration of continuous electrodeionization for removal of heavy metal ions from the primary coolant of a nuclear power plant. *Water Research*. **38**(7):1911–21.

Yoon H, Lee J, Kim S-R, Kang J, Kim S, Kim C, *et al.* (2016). Capacitive deionization with Ca-alginate coated-carbon electrode for hardness control. *Desalination*. **392**:46–53.

Yuan X, Zhang Y, Dong C and Sheng J. (2004). Morphology of ultrafine polysulfone fibers prepared by electrospinning. *Polymer International*. **53**(11):1704–10.

Zadeh ZE, Solouk A, Shafieian M and Nazarpak MH. (2021). Electrospun polyurethane/carbon nanotube composites with different amounts of carbon nanotubes and almost the same fiber diameter for biomedical applications. *Materials Science and Engineering: C*. **118**:111403.

Zheng L, Zhang W, Xiao X. (2016). Preparation of titanium dioxide/tungsten disulfide composite photocatalysts with enhanced photocatalytic activity under visible light. *Korean Journal of Chemical Engineering*. **33**:107–13.

Ziabari M, Mottaghitalab V, Haghi AK. (2010). A new approach for optimization of electrospun nanofiber formation process. *Korean Journal of Chemical Engineering*. **27**:340–54.

Zong X, Kim K, Fang D, Ran S, Hsiao BS and Chu B. (2002). Structure and process relationship of electrospun bioabsorbable nanofiber membranes. *Polymer*. **43**(16):4403–12.

Zuo W, Zhu M, Yang W, Yu H, Chen Y and Zhang Y. (2005). Experimental study on relationship between jet instability and formation of beaded fibers during electrospinning. *Polymer Engineering & Science*. **45**(5):704–9.